Gyrokinetic Simulation of Isotope Effects in Tokamak Plasmas

W. W. Lee

Princeton Plasma Physics Laboratory, Princeton University

P. O. Box 451, Princeton, NJ 08543

and

R. A. Santoro*

Department of Physics, University of California at Irvine

Irvine, CA 92717

()

A three-dimensional (3D) global gyrokinetic particle code in toroidal geometry has been used for investigating the transport properties of ion temperature gradient (ITG) drift instabilities in tokamak plasmas. Using the isotopes of hydrogen (H^+), deuterium (D^+) and tritium (T^+), it is found that, under otherwise identical conditions, there exists a trend for favorable isotope scaling for the ion thermal diffusivity, i.e., χ_i decreases with mass. Such a trend, which exists both at the saturation of the instability and also at the fully nonlinear stage, can be understood from the resulting wavenumber and frequency spectra.

PACS No: 52.65.Tt, 52.52.Fi, 52.35.Qz

*Present Address: Plasma Physics Division, Naval Research Laboratory, Washington, DC 20375

I. INTRODUCTION

The agreement between the recent beam emission spectroscopy and microwave reflectometry measurements of the density fluctuations for the supershot discharges in the Tokamak Fusion Test Reactor (TFTR) [1,2] and the 3D gyrokinetic particle simulation of the ion temperature gradient (ITG) drift instability [3] have not only shown the importance of microturbulence for tokamak confinement but also pointed out the dominant role assumed by the long wavelength ($k_\perp \rho_i < 1$) fluctuations. In this paper, we report on the investigation concerning the effects of these long wavelength modes on thermal transport. More specifically, we have used various hydrogenic isotopes (H^+, D^+, and T^+) in the microturbulence simulation to study the trend for mass scaling and, in turn, to obtain some physical insight concerning the mechanisms responsible for anomalous transport.

Briefly, our simulation results give a favorable mass dependence for χ_i. Although these simulations have been carried out under most idealized conditions and do not contain all the physics of realistic tokamak discharges, they do contain what we believe to be some of the fundamental physics of tokamak plasmas. Therefore, it may not be a coincidence that our mass scaling results are in qualitative agreement with the experimental trend observed in most of the existing tokamaks operated under various confinement scenario, from ohmic to H-mode and supershot discharges. [4] It also seems to agree with the latest L-mode and the ion cyclotron radio frequency (ICRF) heating experiments from TFTR. [5] Since the aim of this paper is to understand the underlying physics for the isotope effects, we have chosen to use a generic toroidal ITG model with no correspondence with any particular machine. In the fully nonlinear stage of the simulation, two important physical characteristics related to the favorable mass scaling have been identified: the widths for both the radial wavenumber spectra and the frequency spectra decrease with mass. The significance of these observations is that one cannot use the prevailing mixing length argument to describe the simulation trend, instead the resonance broadening picture proposed by Dupree [6] seems to give a

better fit.

II. SIMULATION MODEL AND PARAMETERS

In the simulation, we have used the δf scheme for particle pushing, [7,8] for which the original equations of motion for the ion gyrocenters [9] in the gyrokinetic unit of $\rho_s(\equiv \sqrt{T_e/T_i}\rho_i)$ and $\Omega_i(\equiv c_s/\rho_s)$ and $c_s(\equiv \sqrt{T_e/m_i})$ without the nonlinear parallel acceleration can be written as

$$\dot{\mathbf{R}} \equiv \frac{d\mathbf{R}}{dt} = U\hat{\mathbf{b}}^* + \mu\hat{\mathbf{b}} \times (\frac{m_I}{Z_I m_i})\frac{\partial}{\partial \mathbf{R}} lnB + \hat{\mathbf{b}} \times \frac{\partial \overline{\phi}}{\partial \mathbf{R}}, \tag{1}$$

$$\dot{U} \equiv \frac{dU}{dt} = -\hat{\mathbf{b}}^* \cdot \mu \frac{\partial}{\partial \mathbf{R}} lnB, \tag{2}$$

and $\mu/B \equiv v_\perp^2/2B = const.$, where $\hat{\mathbf{b}}^* = \hat{\mathbf{b}} + (m_I/Z_I m_i)U\hat{\mathbf{b}} \times (\hat{\mathbf{b}} \cdot \partial/\partial \mathbf{R})\hat{\mathbf{b}}$ and $\overline{\phi}(\mathbf{R})$ is the finite Larmor radius (FLR) modified potential in unit of e/T_e and can be calculated with the usual 4-point average scheme, [10] and the subscript I denotes species of interest. The "weight" of the particle is given by

$$\dot{w} \equiv \frac{dw}{dt} = -\kappa \frac{\partial \overline{\phi}}{\partial \mathbf{R}} \times \hat{\mathbf{b}} \cdot \hat{\mathbf{r}} - \frac{Z_I T_e}{T_I} U\hat{\mathbf{b}}^* \cdot \frac{\partial \overline{\phi}}{\partial \mathbf{R}}, \tag{3}$$

where $\kappa = \kappa_n - (3/2 - v^2/2v_{tI}^2)\kappa_{TI}$ is the background inhomogeneity resulting from multiple spatial scale expansion and giving rise to a constant external drive (source) in the simulation [10] and $\hat{\mathbf{r}}$ is the unit vector in the minor radius direction. The corresponding δf becomes

$$\delta f = \sum_{j=1}^{N} w_j S(\mathbf{R} - \mathbf{R}_j)\delta(\mu - \mu_j)\delta(U - U_j), \tag{4}$$

where S represents the shape factor for finite-size particles and N is the total number of particles in the simulation. Thus, we are solving the equation

$$(\partial/\partial t + \dot{\mathbf{R}} \cdot \partial/\partial \mathbf{R} + \dot{U}\partial/\partial U)\delta f = \dot{w} f_M \tag{5}$$

in the simulation, where the background Maxwellian f_M is spatially homogeneous. With the assumption that the electron response is adiabatic, i.e., $\delta n_e/n_0 \approx \phi(\mathbf{x})$ (where n_0 is the average number density) and $k_\parallel$ modes are negligible, the gyrokinetic Poisson equation in the Fourier $\mathbf{k}$ space takes the form of

$$[1 + Z_I(T_e/T_I)(1 - \Gamma_0(b_I))]\phi(\mathbf{k}) = \delta\overline{n}_I(\mathbf{k})/n_{0I}, \tag{6}$$

where $Z_I n_{0I} = n_0$, $\Gamma_0 = I_0(b_I)exp(-b_I)$, I_0 is the modified Bessel function and $b_I \equiv (k_\perp \rho_I)^2$. $\delta\overline{n}_I$ is the perturbed number density, $\int \delta f_I dU d\mu$, modified by the FLR effects and can again be calculated by the 4-point average scheme. [10] For simplicity, the self-generated ambipolar field is ignored here, because its effect on the instability is small in a global code. [11] The ion thermal diffusivity in the δf representation can be written as [10]

$$\chi_I \simeq \frac{1}{< \kappa_{TI} > + < \kappa_n >} \sum_{j=1}^{N} -\frac{U_j^2 + 2\mu_j}{v_{tI}^2} w_j \frac{\partial\overline{\phi}}{\partial\mathbf{R}} \times \hat{\mathbf{b}} \cdot \hat{\mathbf{r}}\Big|_{\mathbf{R}_j} /3N, \tag{7}$$

where $< ... >$ represents spatial average.

The simulation has been carried out on a 128x128x64 toroidal grid [a "square" torus model in $(x, y, -R_0\varphi)$ coordinates [3]] with 4.2×10^6 ion gyrocenters (or particles), each with a Gaussian shape for S, where the *rms* particle size is 1.2 grid spacing. Thus, there are 4 particles per cell in the simulation, more than those used in Ref. [3], and the associated numerical convergence property has been studied in Ref. [12]. The toroidal and poloidal magnetic fields are given by $B_t = B_0/(1 + x/R_0)$ and $B_p = rB_0/qR$, respectively, where $q = q_0 + [q_a - q_0](r/a)^2$. The ion temperature gradient is represented by

$$\kappa_{TI} = \kappa_{Ti} = (1/L_{Ti0})sech^2[(r - r_0)/L_w], \tag{8}$$

where the maximum is located at r_0 and L_w is the width of the region with active drive. In the gyrokinetic units of ρ_{sD} and Ω_D^{-1} (i.e., ρ_s and Ω_i^{-1} for the deuterium ions), the other relevant simulation parameters are: $a = 100$, $R_0 = 1000$, $q_0 = 1$, $q_a = 3$, $L_w = 30$,

$r_0 = 55$, $T_e/T_I = 1$, L_n(density scale length) $\equiv 1/\kappa_n = \infty$, and $L_{Ti0} = 100$, $\Delta t = 30$ and $t_{tot} = 200,000$.

III. RESULTS AND INTERPRETATION

The time history of the ITG instability in terms of the gyrokinetic electrostatic field energy, [10] $\sum_k [1 - \Gamma_0(b_i)](T_e/T_i)|e\phi/T_e|^2$, for all three ion species is shown in Fig. 1(a). [In the remainder of the paper, the subscript i denotes the species of interest.] It clearly shows three different stages of the evolution: (I) linear growth and nonlinear saturation ($\Omega_D t = 0 - 3 \times 10^4$), (II) transition period ($\Omega_D t = 3 - 9 \times 10^4$) and (III) fully nonlinear stage ($\Omega_D t = 9 - 20 \times 10^4$). The total energy conservation at the end of the run is about 10^{-4} of the initial kinetic energy, well within the acceptable limit. In the linear stage, which is characterized by the dominance of a few most unstable modes, the trend for the mass dependence of growth rates is consistent with the prediction of $\gamma_L \sim 1/\sqrt{M}$ by Dong et al. [13] The nonlinear saturation level in Fig. 1(a) seems to track the linear growth and, in turn, has similar mass dependence. This is followed by a transition period, where the energy cascade to the longer wavelength modes takes place together with the remnant linear growths of these modes, and the scaling trend seems to reverse. However, the original trend of favorable mass dependence is again restored in the fully nonlinear stage, where the fluctuating field energy stays roughly constant. Figure 1(b) gives the ion thermal diffusivity for all three ion species calculated from Eq. (7), where $L_{Ti} \equiv 1/ < \kappa_{Ti} >$ denotes spatial average and can be calculated from Eq. (8). It has a mass dependence similar to that of the field energy in all three stages of the development. The dominant peaks for χ_i in Fig. 1(b) in stage I are related to the linear growth rates, γ_L, of a few most unstable modes and their associated saturation amplitude, $|\phi|^2$. [The magnitude for χ_i for all three species roughly agrees with the quasilinear estimate of γ_L/k_r^2 [18], when we substitute in the measured values of linear growth from Fig. 1(b) and radial wavenumber from Fig. 2(a), which we will

discuss later.] On the other hand, the fully nonlinear χ_i, which comes from the nonlinear phase difference between the perturbed pressure and potential (along with the fluctuation amplitude), takes some time to achieve. Apparently, the nonlinear phase difference is much smaller than γ_L, resulting in a precipitous drop in χ_i in fully nonlinear state. Nevertheless, Fig 1(b) gives $\chi_i \simeq 0.22(\rho_{sD}/L_{Ti})(cT_e/eB)$ for the deuterium in the fully nonlinear state. When we substitute the parameters for the TFTR perturbed supershot discharge analyzed in Ref. [14], it gives $\chi_i \simeq 2.5m^2/sec$, which compares well with the experimental data taken at the half radius. Thus, we believe our results are very reasonable comparing with our present understanding both at saturation and in the fully nonlinear state. In the remainder of the paper, we will focus on the understanding of the physics of these simulation results and, particularly, the scaling trends in these regions.

To this end, let us first study the radial wavenumber spectra taken at the linear stage just before the saturation as shown in Fig. 2(a). The dominant modes are $m \approx 16, 13, 11$ for H^+, D^+, and T^+, respectively, and are characterized by their ballooning structures. [3] This is the period where k_r is at its minimum. Using the full width half maximum (FWHM) as the reference point, one can see the $k_r \sim 1/M^{1/4}$ dependence for the three species. This is in agreement with the theoretical predictions for the long wavelength toroidal instabilities that the radial structures are prescribed by the equilibrium profile [15] (i.e., L_w in our case) and that, near the maximum gradient, the radial mode widths are proportional to $\rho_i^{1/2} (\sim M^{1/4})$. [16,17] However, near the time of saturation and shortly afterwards, there is a breakup of these spatially coherent structures and the corresponding FWHM wavenumbers become more than doubled. During the ensuing transition period, large amplitude oscillations in k_r take place between these two extremes. In the fully nonlinear state, the amplitude settles to around $\Delta k_r \approx 0.1\rho_{sD}^{-1}$ for $0 \leq k_r \leq 0.5\rho_{sD}^{-1}$ and the time-averaged radial wavenumber spectra during this period of time are shown in Fig. 2(b). Here, the mass dependence for the FWHM wavenumber changes to $k_r \sim 1/M^{1/2}$ with $k_r\rho_s \approx 0.3$. In addition to the active modes observed in the linear stage, lower poloidal harmonics of $m \approx 12, 9, 7$ for H^+,

D^+, T^+, respectively, have also been excited. The corresponding time-averaged k_θ and k_ϕ spectra are shown in Figs. 3(a) and (b), respectively. Unlike the k_r spectra, the poloidal and toroidal wavenumbers don't oscillate much in time in the nonlinear stage. However, all three spectra have the same property, i.e., $k_r\rho_s$, $k_\theta\rho_s(\approx 0.15)$ and $k_\phi\rho_s(\approx 0.6\times 10^{-2})$ are all nearly invariant. In other words,

$$k\rho_s \approx const.$$

in the fully nonlinear stage for all three species, where $\rho_s \sim \sqrt{M}$. Another interesting diagnostic is the frequency spectra in the second half (nonlinear state) of the simulation. Figure 4 shows the spatially averaged spectra along the weak field side of the midplane at a fixed toroidal angle for H^+, D^+, and T^+ plasmas. The results indicate that the nonlinear frequency decreases with mass and, interestingly, so does the frequency spread, $\Delta\omega$. This important property is vital for the understanding of the observed scaling, which we will discuss.

To fully understand the results presented here, one needs a self-consistent nonlinear theory, which is beyond the scope of the present paper. Short of that, let us compare them with some of the present understanding of turbulent transport, e.g., the mixing length argument which gives the scaling of $\chi_i \sim \gamma_L/k_\perp^2$. Since $\omega_{*Ti}/\Omega_i = k_\theta\rho_s^2/L_{Ti}$, one can argue that $\gamma_L/\Omega_i \approx \rho_s/L_{Ti} \sim \sqrt{M}$, if $k_\theta\rho_s$ is invariant. This mass dependence is in agreement with the calculation by Dong et al. [13], which also shows that most unstable toroidal ITG modes occur at $k_\theta\rho_s \approx 0.5$. Thus, we obtain the familiar expression of

$$\chi_i \sim \frac{\rho_s/L_{Ti}}{(k_r\rho_s)^2}\frac{cT_e}{ZeB}. \tag{9}$$

Here, the use of the radial wavenumber k_r for the diffusion can be justified from the quasi-linear theory (see, e.g., Ref. [18]). This scaling can also be obtained from a set of gyrofluid equations based on a simplified Eq. (5) with

$$\dot{\mathbf{R}} \approx U\hat{\mathbf{b}}^* \cdot \hat{\mathbf{y}} + \hat{\mathbf{b}} \times \partial\phi/\partial\mathbf{R},$$

$$\dot{U} \approx 0,$$

$$\dot{w} \approx -\kappa \partial\phi/\partial y - (T_e/T_i) U \hat{\mathbf{b}}^* \cdot \partial\phi/\partial \mathbf{R},$$

$\hat{\mathbf{b}}^* \approx \hat{\mathbf{b}} - (U/R_0)\hat{\mathbf{y}}$, and $\kappa \approx \kappa_n - (1 - U^2/v_{ti}^2)\kappa_{Ti}/2$, where $\hat{\mathbf{b}}$ is in the toroidal direction only. By keeping the first three velocity moments of the equation and ignoring the parallel electric field, these equations give the same Connor-Taylor invariance property [19] as the simple slab equations described in Ref. [18] and Eq. (9) is again a possible solution.

On the other hand, Dupree in a series of papers in the 1960's first proposed the concept of resonance broadening by stating that the wave-particle interaction can be modified by a broadening of the associated resonance denominator $(\omega - \mathbf{k} \cdot \mathbf{v} + i\Delta\omega)^{-1}$ as a result of an incoherent scattering of particle orbits by the waves. This enhanced scattering causes nonlinear saturation of the instability and, in the fully nonlinear state, also causes anomalous diffusion over the transverse wavelength through [6]

$$\Delta\omega \sim k_\perp^2 D. \tag{10}$$

This scattering can be considered as an enhanced viscosity (and can exist when only one single unstable mode is present; see, e.g., Ref. [20]). Equation (10) can also be viewed as the nonlinear version of Eq. (9) in which the linear drive of ρ_s/L_{Ti} is replaced by its nonlinear counterpart, $\Delta\omega/\Omega_i$.

Let us first compare the results for χ_i in Fig. 1(b) with Eq.(9). Based on the measured mass dependence of $k_r \sim 1/M^{1/4}$ from Fig. 2(a) in the linear stage, the quasilinear χ_i should be independent of mass at saturation. Instead, the simulation χ_i's give the ratios of (1.35, 1.75, 1.3) for $(H^+/D^+, H^+/T^+, D^+/T^+)$, which seem to have a $1/\sqrt{M}$ dependence. The implication is that either the linear drive or the radial mode structure is modified. But, neither is true. Since the growth period in the simulation is rather short, particles don't have sufficient time to sample the linear k_r spectra and, therefore, the saturation

level totally depends on the linear growth (i.e., $\chi_i \sim \gamma_L \sim 1/\sqrt{M}$). On the other hand, in the fully nonlinear stage of the simulation, where the simulation time is comparable to or longer than the eddy turnover time, k_r becomes important. [To see this, one can use $\chi_i \approx (\Delta x)^2/(2\Delta t)$ to estimate the average step size and compare it with the typical eddy size from the k_r spectra in Fig. 2.] Here, the time-averaged ratios for χ_i are (1.3, 1.8, 1.4) for $(H^+/D^+, H^+/T^+, D^+/T^+)$, which have similar dependence on mass as the quasilinear χ_i's in the simulation. Substituting the results from Fig. 2(b) of $k_r \sim 1/\sqrt{M}$ (i.e., $k_r\rho_s \approx const.$) into Eq. (9), one finds $\chi_i \sim \sqrt{M}$, which gives an opposite scaling. One obvious explanation is that, in the fully nonlinear state, the linear drive becomes meaningless. One should then use Eq. (10) instead, i.e., replacing the linear drive in Eq. (9) by a nonlinear one. Fig. 4 provides just that and indicates that the fluctuations are less coherent with higher frequencies for lighter isotopes, i.e., $\Delta\omega/\Omega_i$'s are larger. (Note that there is nonlinear downward frequency shift since $\omega/\Omega_D \simeq 0.001$ in the linear stage for all three species.) This in-coherency is apparently related to the differences in fluctuation amplitude of the electrostatic field energy for the three isotopes as shown in Fig. 1(a), and is consistent with the prediction from the $E \times B$ de-correlation (or trapping) rate of $\omega_{EB}/\Omega_i \simeq 4k_r\rho_s k_\theta \rho_s e\phi/T_e$ in the fully nonlinear stage. The broadening is further enhanced by the fact that the linearly unstable region in k_θ is much broader for lighter isotopes, as shown in Fig. 1 of Ref. [13]. Therefore, a global simulation code such as ours, which takes into account the spatial variation of the temperature gradient, is best suited for capturing the relevant physics in these cases. The comparison of $\Delta\omega$ in Fig. 4 can be carried out again by using FWHM. Noting that part of $\Delta\omega$ comes from the fast Fourier transform (FFT) sampling error, $2\pi/t_{tot}$, one can show that $\Delta\omega_H/\Delta\omega_T \approx 5$ and Eq. 10 [i.e., Eq. (9) with the nonlinear drive, $\Delta\omega/\Omega_i$], gives $\chi_i^H/\chi_i^T \approx 1.7$ which is consistent with the simulation results of

$$\chi_i \sim 1/\sqrt{M}.$$

To further explore the relationship between the mixing length argument and the reso-

nance broadening estimate, let us now turn our attention to the interesting case of helium-4, H_{e4}^{2+}, which has the same ρ_s ($Z_{He}/Z_H = 2$, $m_{He}/m_H = 4$) as hydrogen. Simulations for these two species have been carried out again using Eqs. (1) - (7) with the same number (4.2×10^6) of particles as before, but with slightly different initial conditions and shorter simulation time. (It should be pointed out here that the proper concentration of helium-4 ions in relation to the background electrons to maintain quasineutrality has also been taken into account.) The results are shown in Fig. 5. The time evolution for the two species has a very similar feature for the field energy as well as for the ion thermal diffusivity, (and is also similar to the results in Fig. 1). One may ascertain that both $|\phi|^2$ and χ_i scale roughly as $1/Z$ in the fully nonlinear stage ($\Omega_D t = 10 - 15 \times 10^4$). To understand the implication of this scaling for thermal diffusivity, let us start with the mixing length argument, $\chi_i \sim \gamma_L / k_\perp^2$. Assuming $(k_r \rho_s)^2 \sim (\rho_s / L_{Ti})^\alpha$, we can re-write Eq. (9) as

$$\chi_i \sim (\rho_s / L_{Ti})^{1-\alpha} (cT_e / ZeB). \tag{11}$$

Thus, $\alpha = 0$ or 1 gives rise to a gyro-Bohm or Bohm scaling, respectively. Because $\rho_*(\equiv \rho_s / L_{Ti})$ is the same for the two cases, thermal diffusivities for hydrogen and helium-4, according to this estimate, should scale only like $1/Z$ for arbitrary α. This is in rough agreement with the simulation results and it seems to be due to the fact the scaling here is independent of ρ_s / L_{Ti}. Nevertheless, this is a very special case where the mixing length argument is actually applicable. But, in general, this is not true when ρ_s / L_{Ti} scaling is involved, as we have demonstrated earlier. As for resonance broadening, Eq. (10) for $k_r \rho_s \approx const.$ gives

$$\chi_i \sim \frac{\Delta\omega}{\Omega_i} \frac{cT_e}{ZeB} = \frac{\Delta\omega}{\Omega_H} \frac{A}{Z^2} \frac{cT_e}{eB},$$

where A is the atomic mass number and $A/Z^2 = 1$ in this case. Thus, χ_i depends only on nonlinear frequency shift. The measured nonlinear frequency broadening for H_{e4}^{2+} is indeed smaller and, in turn, gives a smaller χ_i for helium-4. Therefore, this scaling is also consistent

with the simulation results in Fig. 5(b). It should also be mentioned here that, since the amplitude for the potential fluctuation, $|\phi|$, is smaller for helium-4 than for hydrogen as indicated by Fig. 5(a), it is not surprising that the corresponding $\Delta\omega$ for helium-4 is smaller than the nonlinear frequency spread for hydrogen.

IV. CONCLUSION AND DISCUSSION

In this paper, we have demonstrated the existence of favorable isotope scaling for ion temperature gradient drift instabilities using a three-dimensional global gyrokinetic particle code. [3] We have also compared our results in the fully nonlinear stage of the development with the mixing length argument and with the resonance broadening estimate. It is found that the mixing length argument, Eqs. (9) and (11), is inadequate for predicting such a scaling, apparently because the argument is based on the linear drive prescribed only by local parameters. On the other hand, resonance broadening estimate based on the nonlinear frequency spread, $\Delta\omega$, seems to describe accurately the scaling of χ_i in the fully nonlinear stage of the simulation. This, we believe, is because such an estimate is better for capturing the global nature of the ITG turbulence. Specifically, we have found that a lighter isotope involves more unstable modes with a higher level of fluctuation than that of a heavier one. The higher fluctuation, in turn, gives rise to a larger nonlinear frequency broadening due to $E \times B$ detrapping. The stability diagram of Fig. 1 in Ref. [13] indicates that H^+ not only has higher growth rates but also has more unstable modes than D^+ and this is also true for D^+ in comparison with T^+. This linear property apparently manifests itself in our nonlinear results as well. Our global code is also capable of capturing the physics associated with the spatial variation of the temperature gradient. Furthermore, we have found that $k\rho_s \simeq const.$ in the fully nonlinear stage of the simulation in all three (r, θ, ϕ) dimensions. Thus, the wavelengths for the perturbation scale with the gyroradius of the species rather than with the minor radius a. This desirable feature is usually associated with the gyro-

Bohm scaling, as we have mentioned earlier. From Dupree's resonance broadening picture, Eq. (10), [6] we argue that these properties of $k_r\rho_s$ and $\Delta\omega$ can give us the favorable isotope scaling. To identify the non-local dimensionless parameters which characterize this type of resonance broadening scaling is an important task for us all in the future. Most of all, we need a sound theoretical understanding of microturbulence.

ACKNOWLEDGMENT

The authors would like to thank Drs. S. E. Parker and J. C. Cummings for discussions and assistance in the GET3D code. Interactions with Drs. T. S. Hahm and L. Chen are also gratefully acknowledged. The present work is supported by the U.S. Department of Energy under Contract No. DE-AC02-76-CHO3037 and Grant No. DE-FG03-94ER54271. The Cray C90 at the National Energy Research Supercomputer Center has been used for the simulation.

REFERENCES

[1] R. J. Fonck, G. Cosby, R. D. Durst, S. F. Paul, N. Bretz, S. Scott, E. Synakowski and G. Taylor, Phys. Rev. Lett. **70**, 3736 (1993).

[2] E. Mazzucato and R. Nazikian, Phys. Rev. Lett. **71**, 1840 (1993).

[3] S. E. Parker, W. W. Lee, and R. A. Santoro, Phys. Rev. Lett. **71**, 2042 (1993).

[4] M. Bessenrodt-Weberpals, F. Wagner and ASDEX Team, Nuclear Fusion **33,** 1205 (1993).

[5] R. Majeski, J. H. Rogers, S. H. Batha, A. Bers, R. Budny, D. Darrow, H. H. Duong, R. K. Fisher, C. B. Forest, E. Fredrickson, B. Grek, K. Hill, J. C. Hosea, D. Ignat, B. LeBlanc, F. Levinton, S. S. Medley, M. Murakami, M. P. Petrov, C. K. Phillips, A. Ram, A. T. Ramsey, G. Shilling, G. Taylor, J. R. Wilson and M. C. Zarnstorff, Phys. Plasmas **3**, 2006 (1996).

[6] T. H. Dupree, Phys. Fluids **11**, 2680 (1968).

[7] A. M. Dimits and W. W. Lee, J. Comput. Phys. **107**, 309 (1993).

[8] S. E. Parker and W. W. Lee, Phys. Fluids B **5**, 77 (1993).

[9] T. S. Hahm, Phys. Fluids **31**, 2670 (1988).

[10] W. W. Lee, J. Comput. Phys. **72**, 243 (1987).

[11] J. C. Cummings, Ph.D. thesis, Princeton University, 1995.

[12] S. E. parker, H. E. Mynick, M. Artun, J. C. Cummings, V. Decyk, J. V. Kepner, W. W. Lee, and W. M. Tang, Phys. Plasmas **3** 1959 (1996).

[13] J. Q. Dong, W. Horton, and W. Dorland, Phys. Plasmas **1**, 3635 (1994).

[14] W. Horton, D. Lindberg, J. Y. Kim, J. Q. Dong, G. W. Hammett, S. D. Scott, M.

Zarnstorff, and S. Hamaguchi, Phys. Fluids B **4**, 953 1992).

[15] W. M. Tang and G. Rewoldt, Phys. Fluids B **5**, 2451 (1993).

[16] F. Romanelli and F. Zonca, Phys. Fluids B **5**, 4081 (1993).

[17] T. S. Hahm and W. M. Tang, Phys. Plasmas **3**, 242 (1996).

[18] W. W. Lee and W. M. Tang, Phys. Fluids **31**, 622 (1988).

[19] J. Connor, Nucl. Fusion **26**, 193 (1986).

[20] W. W. Lee, J. Krommes, C. Oberman, and R. Smith, Phys. Fluids **27**, 2652 (1984).

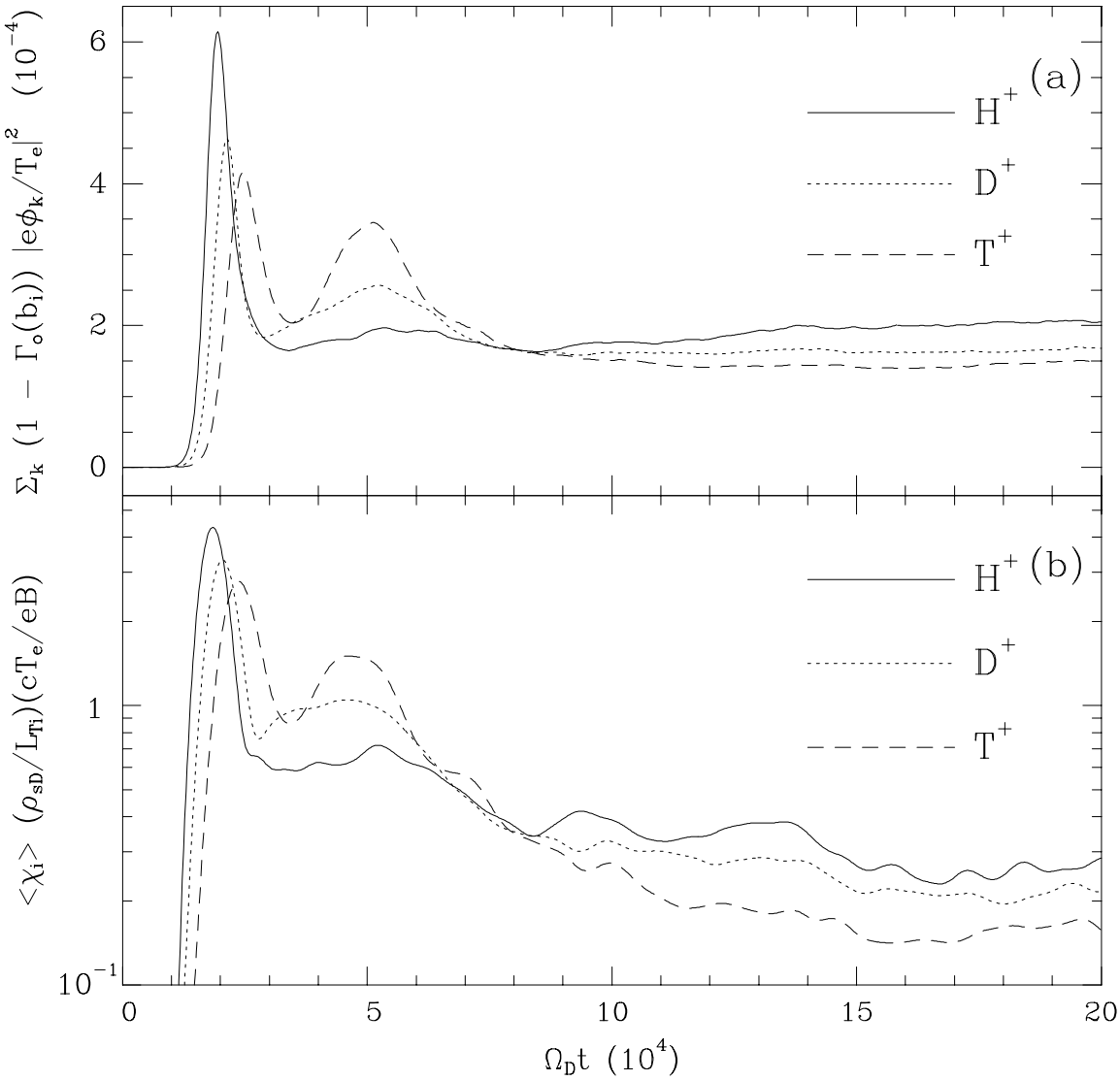

FIG. 1. Time evolution for the ITG instability for the three hydrogenic isotopes in terms of the electrostatic field energy (a) and the ion thermal diffusivity (b), where subscript D denotes deuterium.

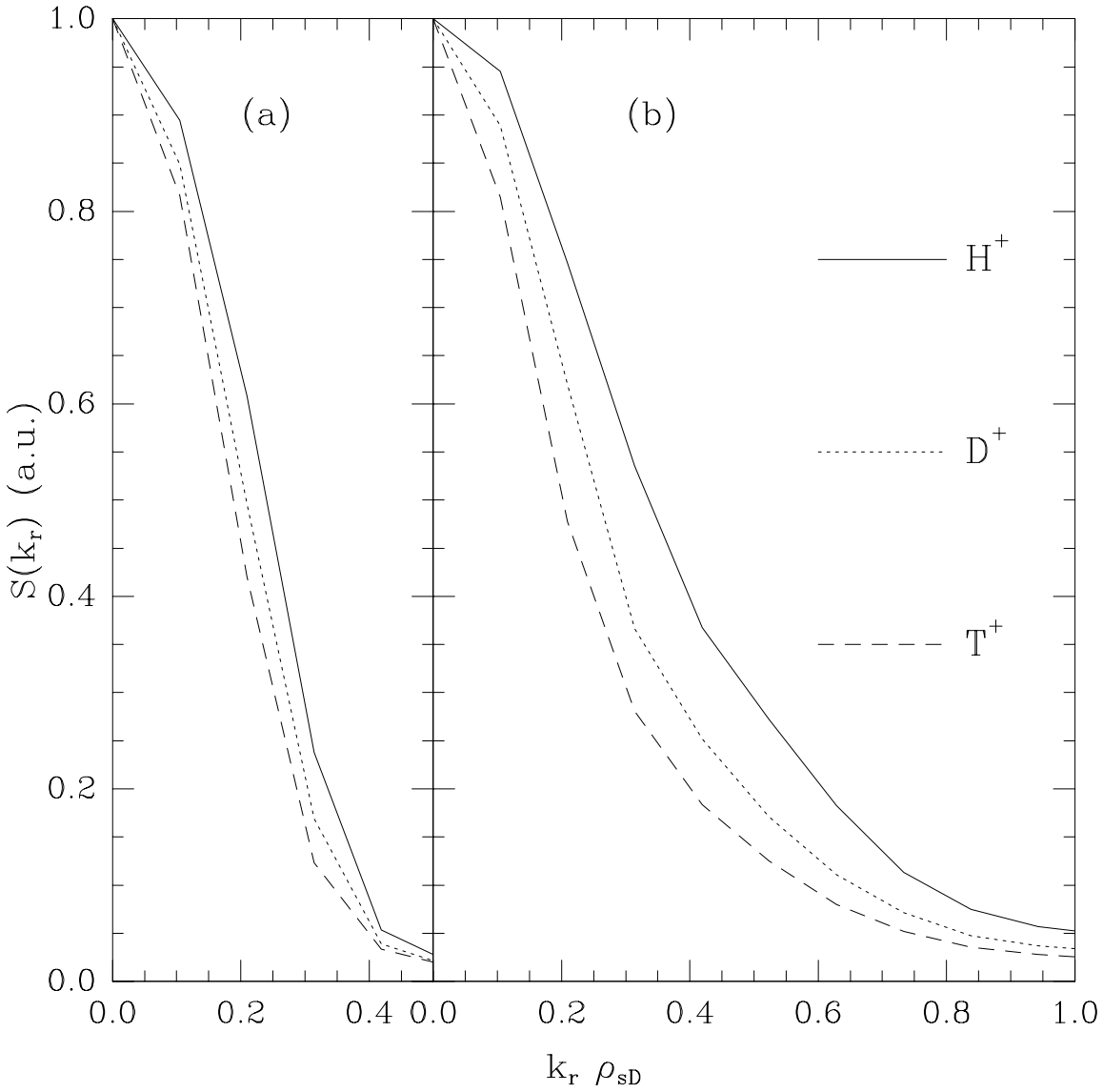

FIG. 2. The linear radial wavenumber k_r spectra (a) and the time-averaged k_r spectra in the fully nonlinear state (b), where subscript D denotes deuterium.

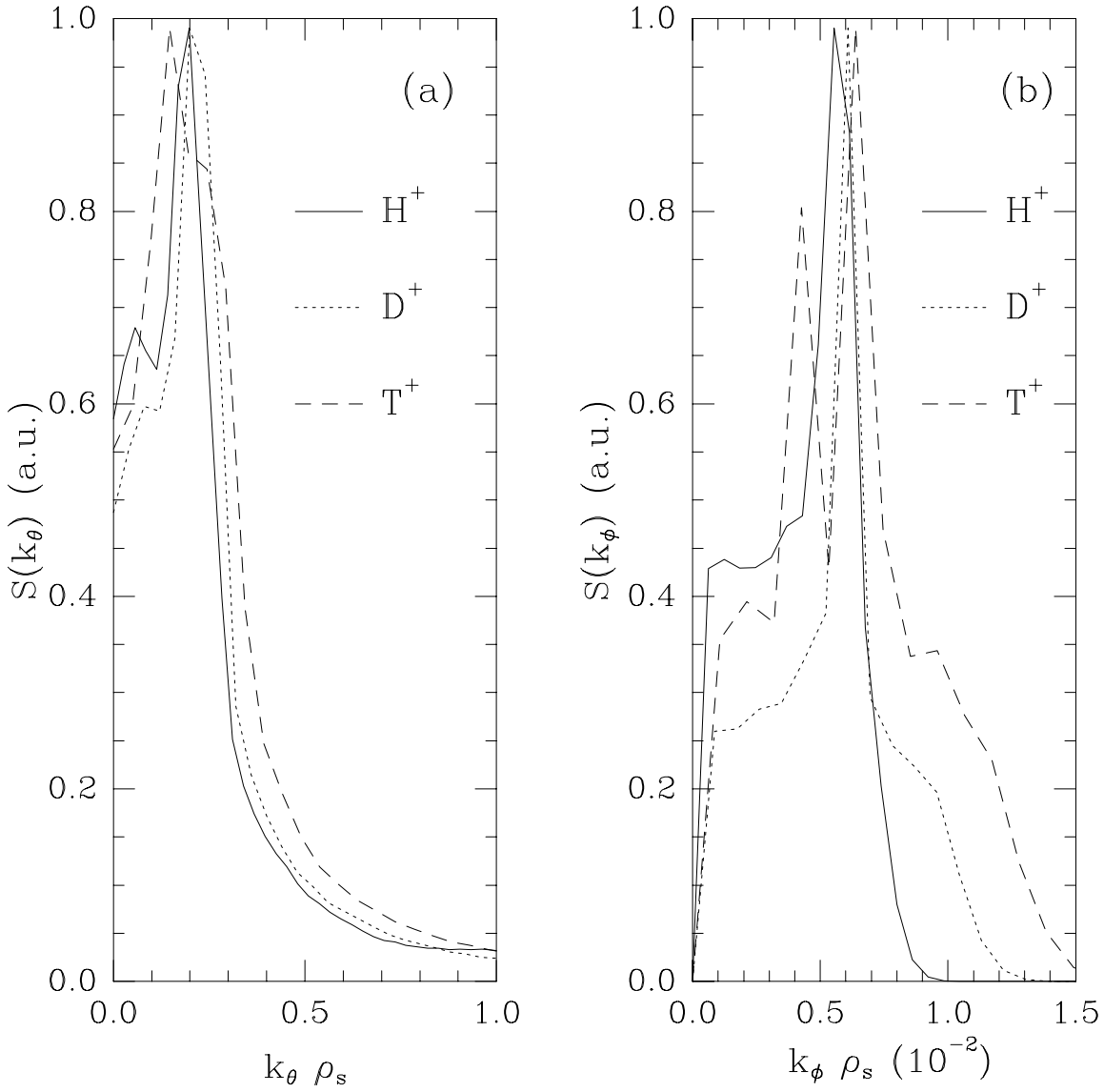

FIG. 3. The time-averaged poloidal k_θ spectra (a) and toroidal k_ϕ spectra (b) in the fully nonlinear state, where ρ_s is mass dependent.

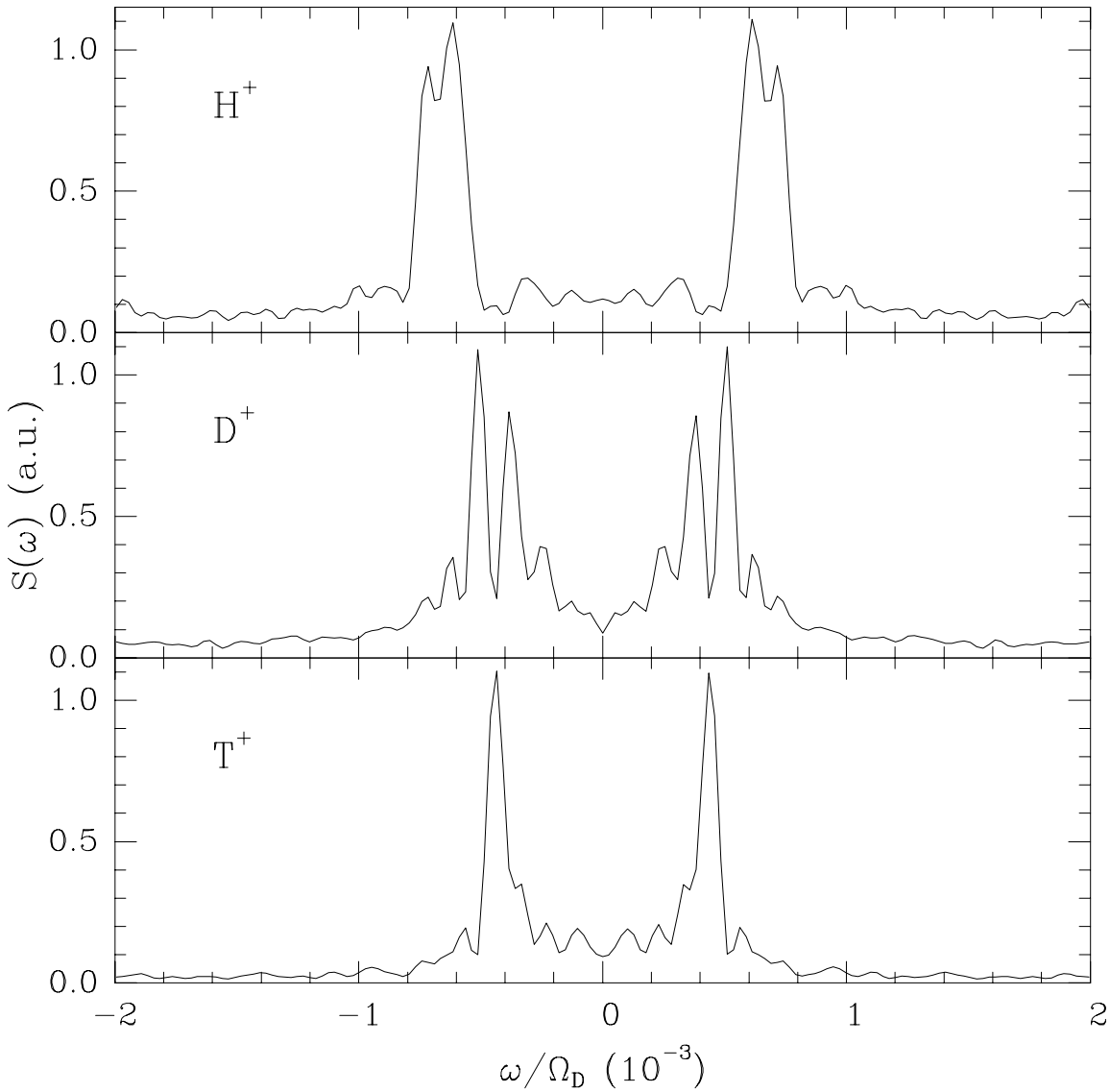

FIG. 4. Spatially-averaged frequency spectra along the weak magnetic field side of the midplane for the three hydrogenic isotopes, where subscript D denotes deuterium.

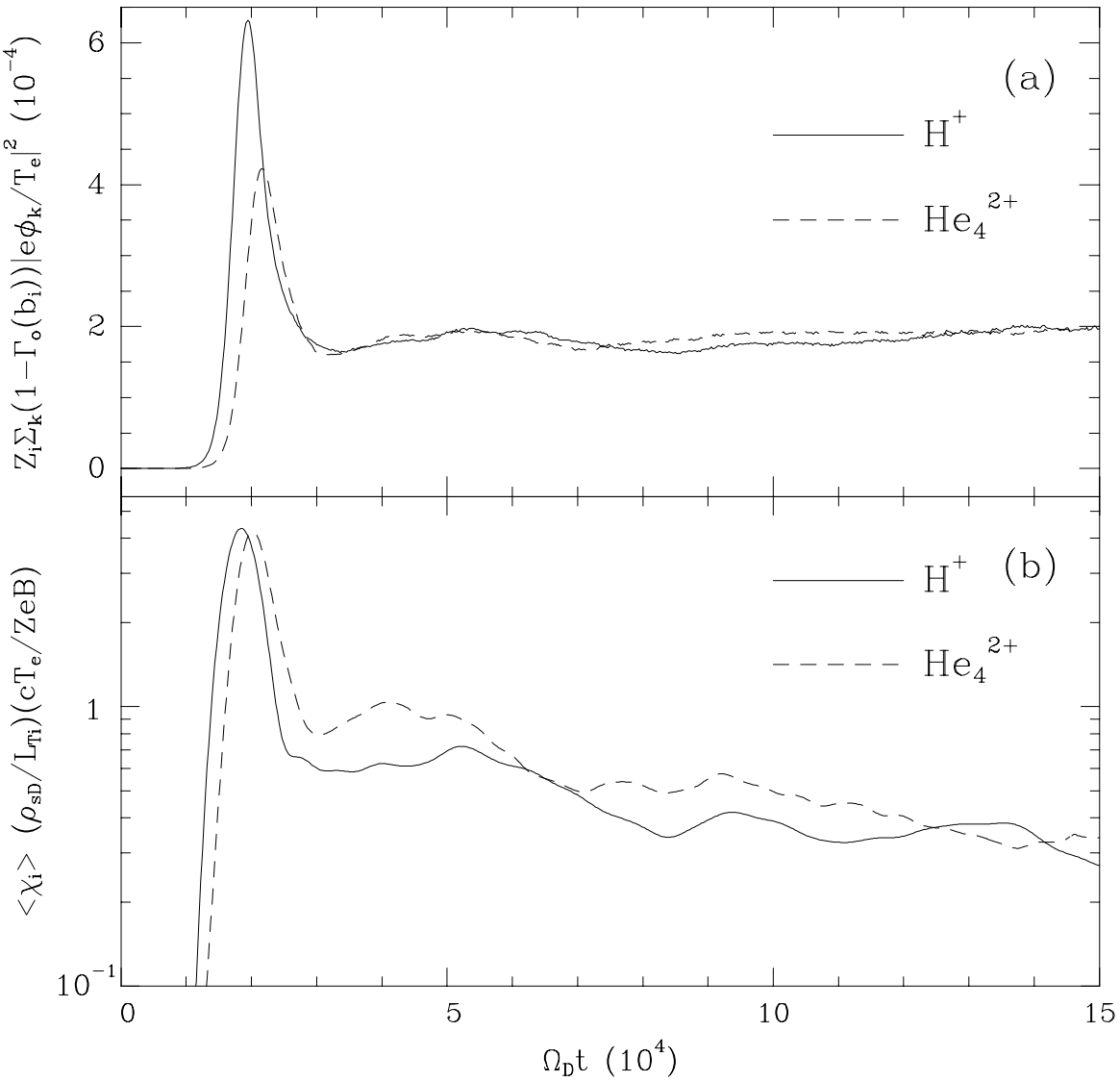

FIG. 5. Time evolution for the ITG instability for hydrogen and helium-4 in terms of field energy (a) and the ion thermal diffusivity (b), where subscript D denotes deuterium.